High supersaturation inside cirrus in well-developed tropical tropopause layer over Indonesia

Y. Inai,[1,2] T. Shibata,[1] M. Fujiwara,[3] F. Hasebe,[3] and H. Vömel[4]

Received 22 August 2012; revised 20 September 2012; accepted 28 September 2012; published 27 October 2012.

[1] The relationship between relative humidity and cirrus clouds in the tropical tropopause layer (TTL) is investigated using balloon-borne cryogenic frostpoint hygrometers (CFH) and quasi-collocated measurements of space-borne Cloud-Aerosol Lidar with Orthogonal Polarization (CALIOP) over Biak (1.17°S, 136.06°E) and Kototabang (0.20°S, 100.32°E) both in Indonesia in Januaries 2007 and 2008. At Kototabang, thin layers of high supersaturation, up to ∼160% in relative humidity with respect to ice (RHi), are often observed co-existing with cirrus clouds at altitudes of ∼15–18 km. At Biak, RHi inside cirrus is around 100% or less without large supersaturation layers, and most clouds are limited to altitudes below 16 km. We found that the presence and the degree of supersaturation may strongly depend on the phases of large-scale disturbances such as the MJO rather than geographical difference. **Citation:** Inai, Y., T. Shibata, M. Fujiwara, F. Hasebe, and H. Vömel (2012), High supersaturation inside cirrus in well-developed tropical tropopause layer over Indonesia, *Geophys. Res. Lett.*, *39*, L20811, doi:10.1029/2012GL053638.

1. Introduction

[2] The amount of stratospheric water vapor is largely controlled by dehydration processes in the tropical tropopause layer (TTL). A dehydration process associated with horizontal advection (cold trap dehydration) is considered to be the key process in the TTL [*Holton and Gettelman*, 2001; *Hatsushika and Yamazaki*, 2003] and works most efficiently over the Indonesian maritime continent during the boreal winter; this is where and when the TTL is coldest and when cirrus clouds are most frequently observed in the TTL [e.g., *Wang et al.*, 1996; *Massie et al.*, 2010]. Y. Inai et al. (Dehydration in the tropical tropopause layer estimated from the water vapor match, manuscript in preparation, 2012) suggested that dehydration associated with horizontal advection is efficient at least in the lower part of the TTL but that efficiency at the critical altitude where the entry value of water vapor mixing ratio is controlled by dehydration is still unknown.

[3] TTL cirrus provide evidence that dehydration is occurring [*Holton and Gettelman*, 2001]. However, the microphysical processes involved are unclear [*Peter et al.*, 2006]. *Shibata et al.* [2007] studied the relationship between cirrus and supersaturation over Indonesia using ground-based lidar measurements and balloon-borne cryogenic frostpoint hygrometers (CFH). *Fujiwara et al.* [2009] showed variations of cirrus and relative humidity over the western Pacific using ship-borne lidar and sondes launched with a 3-hourly frequency. However, the former analyzed only a few cases, and the latter was based mostly on operational radiosonde for water vapor measurements. *Krämer et al.* [2009] summarized observed supersaturation and the presence or absence of cirrus clouds for the TTL and upper troposphere and lower stratosphere. They analyzed water vapor data from aircraft measurements in three tropical regions but the regions driving the cold trap dehydration most efficiently (i.e., the western tropical Pacific in northern winter) were not included. Collocated measurements of water vapor, temperature, and cirrus clouds are essential for understanding cloud microphysics and dehydration in the TTL and stratospheric water vapor variation.

[4] This study analyzes balloon-borne CFH data taken at Biak (1.17°S, 136.06°E) and Kototabang (0.20°S, 100.32°E), in January 2007 and in January 2008, during the Soundings of Ozone and Water in the Equatorial Region (SOWER) campaigns [e.g., *Fujiwara et al.*, 2010], and space-borne Cloud-Aerosol Lidar with Orthogonal Polarization (CALIOP) data [*Winker et al.*, 2007]. Water vapor and cirrus cloud distributions in our target region are largely affected by various types of tropical disturbances such as the Madden-Julian Oscillation (MJO) and Kelvin waves [*Eguchi and Shiotani*, 2004; *Fujiwara et al.*, 2009, and references therein]. We will investigate the relationship among relative humidity, cirrus clouds, and large-scale disturbances in the TTL.

2. Data and Methods

[5] Water vapor mixing ratio is measured by the CFH, a balloon-borne chilled-mirror hygrometer [*Vömel et al.*, 2007]. The uncertainty of CFH measurements is estimated to be less than 9% of the mixing ratio in the TTL [*Vömel et al.*, 2007]. Note that the uncertainty is virtually not affected by the presence or absence of cirrus cloud particles because of the measurement principle and our quality control. The CFH was launched with a Vaisala RS80 radiosonde and an electrochemical concentration cells (ECC) ozonesonde. The uncertainty of RS80 temperature measurements is 0.2 K [*Vaisala*, 1997] corresponding to ∼3–4% of the mixing ratio in the TTL. Effective vertical resolution of balloon-borne temperature and water vapor data is about <13 m and <100 m, respectively. The numbers of successful soundings are as follows: 6 and 7 at Biak in January 2007 and 2008, respectively, and 4 and 4 at Kototabang in January 2007 and 2008,

[1]Graduate School of Environmental Studies, Nagoya University, Nagoya, Japan.
[2]Now at Graduate School of Science, Tohoku University, Sendai, Japan.
[3]Faculty of Environmental Earth Science, Hokkaido University, Sapporo, Japan.
[4]GRUAN Lead Center, Lindenberg, Germany.

Corresponding author: Y. Inai, Graduate School of Science, Tohoku University, Sendai 980-8578, Japan. (yinai@caos-a.geophys.tohoku.ac.jp)

0094-8276/12/2012GL053638

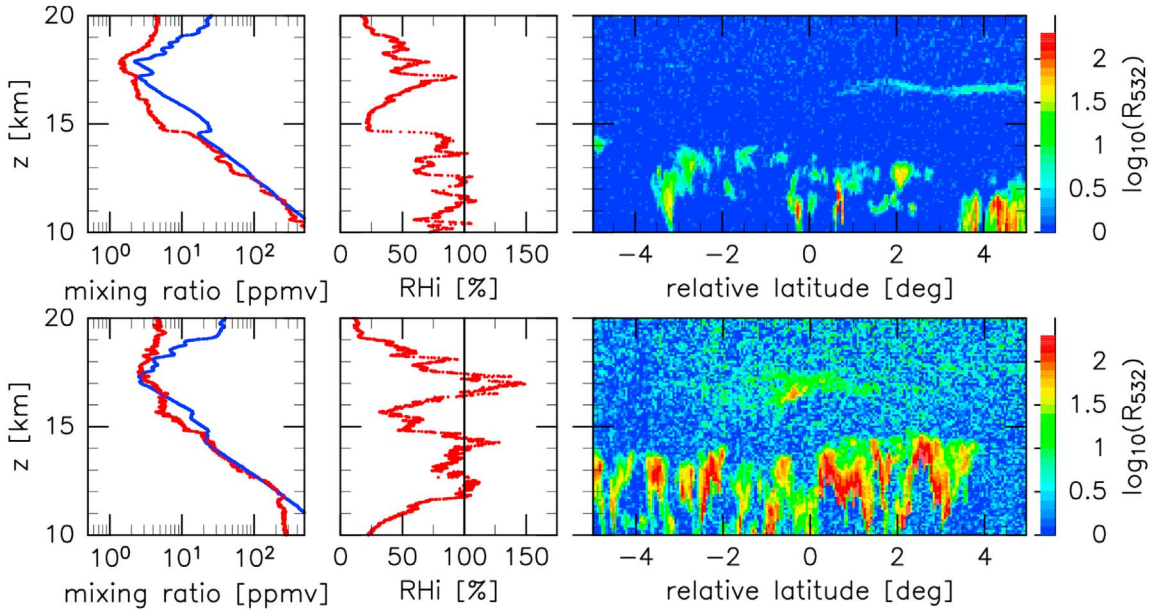

Figure 1. Examples of collocated measurements (top) at Kototabang on January 9, 2008 (23:59 UTC for CFH and 19:18 UTC at 0° relative latitude for CALIOP; the longitude difference between the two measurements is 3.92°) and (bottom) at Kototabang on January 11, 2007 (01:42 UTC for CFH and 07:15 UTC at 0° relative latitude for CALIOP; the longitude difference between the two measurements is 3.02°). (left) Vertical profiles of saturation water vapor mixing ratio (blue) and water vapor mixing ratio (red). (middle) Relative humidity over ice (red). (right) Latitude-altitude distribution of backscattering ratio R_{532} (color) along the CALIOP track (the latitude is relative to the CFH launch site).

respectively. Water vapor and ozone mixing ratios are sensitive to air pressure, so pressure data should be corrected as much as possible. These data are corrected using the comparison between the height calculated from integrating the hypsometric equation and simultaneous Global Positioning System height measurements in the CFH following *Inai et al.* [2009]. The frost-point temperature measured by CFH is converted to water vapor pressure using the Goff-Gratch equation [*Goff and Gratch*, 1946; *List*, 1984].

[6] CALIOP onboard Cloud- Aerosol Lidar and Infrared Pathfinder Satellite Observation (CALIPSO) has measured cloud backscatter from June 2006 to the present. High vertical resolutions are utilized in the level 1 v3.01 products of the CALIOP backscattering data. The vertical resolution of these products is about 60 m. The horizontal interval of the original CALIOP data along its orbit is 330 m. We use a 15-point running average to reduce noise; thus, effective horizontal resolution is ~5 km along the orbit in this study. This resolution may be too coarse to resolve isolated convective clouds but fine enough to describe TTL cirrus (~10–100 km or more according to *Massie et al.* [2010]) and meso-scale convective systems.

[7] To detect cirrus clouds, the backscattering ratio at 532 nm,

$$R_{532} = \frac{\beta_1 + \beta_2}{\beta_2} \quad (1)$$

is used. β_1 and β_2 are backscattering coefficients at 532 nm for atmospheric particles and molecules, respectively. β_2 is derived from Global Modeling and Assimilation Office (GMAO) meteorological data and β_1 is calculated using the algorithm proposed by *Fernald* [1984] with the 18.0 sr lidar ratio (extinction to backscatter) for cloud particles.

[8] *Massie et al.* [2010] estimated the scale of TTL clouds in a meridional direction as ~10–100 km or more. The criteria for the collocation, i.e., acceptable temporal-spatial difference between CFH and CALIOP measurements are determined practically to be within 6 hours and 5° longitude (~560 km) in this study. This scale is smaller than those of the cold trap dehydration process, which is ~1000 km [*Holton and Gettelman*, 2001; *Hatsushika and Yamazaki*, 2003], as well as large-scale disturbances in the TTL. Horizontal winds at 25 m s^{-1}, which may be typical in the TTL, transport air mass for 560 km in ~6 hours. These criteria were chosen after a sensitivity study, where the results were examined by changing the criteria from 2.5 degree to 10.0 degree in longitude and from 3 hours to 24 hours in time. It was confirmed that the results did not depend largely on the longitude values between 2.5° and 5.0°. These criteria have chosen to ensure enough sampling number for this analysis. Note that we do not specify the latitudinal criterion because the CALIPSO is a polar-orbit satellite. For each CFH profile, there are usually several CALIOP profiles which satisfy the above criteria; we chose the temporally closest one as the collocated CALIOP profile.

3. Results

3.1. Water Vapor Profiles and Collocated Lidar Echoes

[9] Figure 1 (top) shows an example of CFH and collocated CALIOP measurements over Kototabang on January 9, 2008. The profiles of saturation water vapor mixing ratio, water vapor mixing ratio, and relative humidity over ice (RHi) are measured by CFH. The latitude-height section of R_{532} is

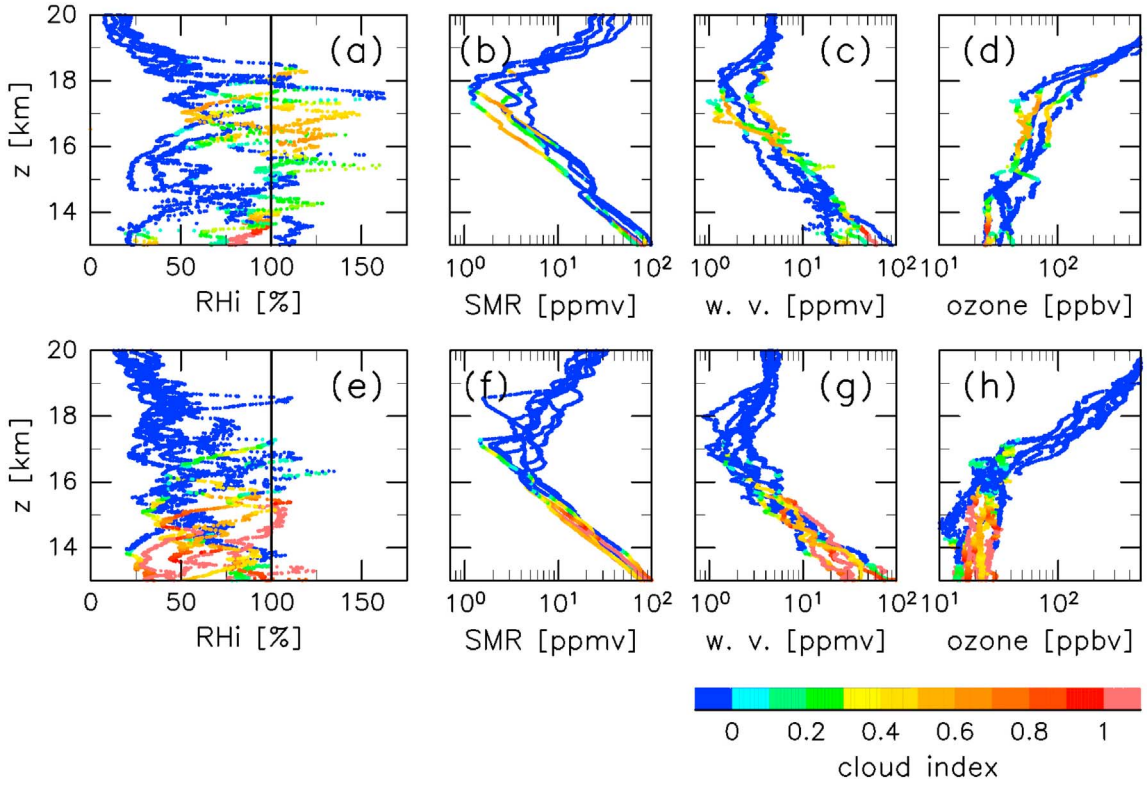

Figure 2. Vertical profiles of (a, e) RHi, (b, f) saturation water vapor mixing ratio, (c, g) water vapor mixing ratio, and (d, h) ozone mixing ratio for all the collocated measurements at Kototabang (Figures 2a–2d) and at Biak (Figures 2e–2h). The color shows the 10-base logarithm of backscattering ratio to the cloud threshold value (i.e., the cloud index defined by Equation (3)) calculated from CALIOP data.

measured by CALIOP. The latitude range is ±5° centered at the latitude of the CFH launch site (lat_{CFH}). The temporal and spatial observational lags between CALIOP and CFH are 4.7 hours (CALIOP earlier) and −3.92° longitude (CALIOP minus CFH), respectively. Below 14 km altitude, small-scale cloud systems exist at a horizontal scale of ∼100 km. In the same altitude region, the RHi profile has some saturated layers. The altitude range 15–17 km is cloud-free and very dry with a minimum RHi of less than 25%. At about 17 km, CALIOP found a laminar cirrus layer on the northern side of the CFH launch station and the CFH measurement showed a thin humid layer at the corresponding altitude.

[10] Figure 1 (bottom) shows measurements over Kototabang on January 11, 2007, including a high supersaturation within cirrus clouds in the TTL. The CALIOP measurements are somewhat noisy due to solar radiation contamination in daytime [e.g., *Wu et al.*, 2011]; therefore, R_{532} values are subject to a certain amount of noise (see Figure 1, bottom right). Nonetheless, a cirrus cloud can be seen in the CALIOP measurement at around 17 km and the same layer shows supersaturation with RHi up to 150% in the CFH measurement. Below 15 km, there are some saturated layers with more clouds than in the top panel of Figure 1 but they are separated from the cirrus cloud in the TTL by a very dry layer of ∼2 km thick, similar to that in the top panel.

3.2. Sonde-Observed Profiles Combined With Cloud Information for All Cases

[11] Most other cases of collocated measurements for Kototabang and Biak also show that the humid layers, in which RHi exceeds 100%, contain cirrus clouds in the TTL. The average profiles of the collocated CALIOP backscatter signals are calculated for each collocated measurements. The averages of β_1 ($\equiv\bar{\beta}_1(z)$) and β_2 ($\equiv\bar{\beta}_2(z)$) are calculated for each altitude z within the latitude range $lat_{\mathrm{CFH}} \pm 1°$. It should be noted that the background noise in the CALIOP data is very different for different orbits, especially between daytime and nighttime measurements (described in previous subsection); thus, it is not appropriate to use R_{532} directly. Instead, the mean background backscatter coefficient produced by noise ($\equiv\bar{\beta}_{noise}$) and its standard deviation ($\equiv \sigma_{noise}$) are calculated from β_1 at 19–20 km within $lat_{\mathrm{CFH}} \pm 1°$ for each profile. In this $\bar{\beta}_{noise}$ calculation, it is assumed that the air mass at 19–20 km has no particles. To determine the cloud signal, a threshold value $\beta_{th}(z)$ is defined as

$$\beta_{th}(z) = \bar{\beta}_2(z) + \bar{\beta}_{noise} + 3\sigma_{noise}, \tag{2}$$

for all analysis altitudes (13.5–20 km), and the altitude where the value of $\bar{\beta}_1(z) + \bar{\beta}_2(z)$ becomes greater than that of $\beta_{th}(z)$ is regarded as cloud. In other words, if the cloud index,

$$\text{cloud index}(z) = \log_{10}\left(\frac{\bar{\beta}_1(z) + \bar{\beta}_2(z)}{\beta_{\mathrm{th}}(z)}\right) \tag{3}$$

becomes positive, the region is defined as cloud. Efficacy of this definition is confirmed in both daytime and nighttime observations.

[12] Figure 2 shows vertical profiles of RHi, saturation water vapor mixing ratio, water vapor mixing ratio, and

Table 1. Summary of the Measurement Results

Station (lat., lon.)	# of Collocated Cases	# of Cases RHi > 100%	# of Cases RHi > 125%	Altitude Range of Cirrus	TTL Thickness
Kototabang (0.20°S, 100.32°E)	5	5	3	15.2–18.3 km and below 14.5 km	∼3 km
Biak (1.17°S, 136.06°E)	7	6	1	up to 17.2 km	<1 km

ozone mixing ratio; colors show the cloud index of each collocated cirrus measurement at Kototabang and Biak. There are five collocated cases for Kototabang and seven for Biak. Local times of sonde measurements are 08:01, 08:42, 07:00, 06:37, and 07:06 at Kototabang, and 14:35, 14:17, 14:06, 23:06, 12:25, 23:18, and 18:46 at Biak.

[13] Figure 2 shows that many high supersaturation cases occur at altitudes up to ∼18.3 km at Kototabang, co-existing with cirrus clouds. All soundings have supersaturated layers and three out of five have a high supersaturated layer exceeding 125% RHi. RHi reaches a maximum of ∼160% at the cold point level measured on January 13, 2008. These RHi profiles have sharp peaks (typically about 1 km thickness) with cloud signals. Cirrus clouds exist just below the cold point altitude and water vapor mixing ratio minimum. Final dehydration is likely to take place at this altitude, determining the entry value of water vapor mixing ratio for the stratosphere. Ozone profiles show a steep gradient above ∼17.5 km and relatively low values below ∼14.5 km. The profiles of saturation water vapor mixing ratio (i.e., temperature) and ozone mixing ratio suggest that the altitude range from ∼14.5–17.5 km is the TTL.

[14] At Biak, RHi is lower than at Kototabang; six soundings have supersaturated layers but only one out of seven has a high supersaturated layer exceeding 125% RHi. The cloud signals appear at altitudes up to ∼17.2 km but many cloud signals and high values of cloud index exist only below 16 km altitude. Ozone shows a steep gradient above ∼16.5 km and low concentrations below this level, suggesting that the region just above ∼16.5 km is stratosphere and below this altitude is highly convective troposphere; in other words, the TTL is very thin. A summary of the findings at the two stations are shown in Table 1.

4. Discussion

[15] As described in the previous section, different features between Kototabang and Biak are found. These two sites are located at the western and eastern part of the maritime continent, respectively. However, the microphysical property of cirrus clouds may depend on meteorological conditions (i.e., the phases of large-scale disturbances) rather than the geographical difference as discussed below. In general, high supersaturation can be maintained in an environment in which ice crystal number density is low. According to previous studies, assuming slower cooling rates results in fewer ice crystals nucleating and less competition for vapor [e.g., *Jensen et al.*, 2008]. Here, the meteorological fields that produce the different aspects between Kototabang and Biak shown in Figure 2 for both campaign periods (in Januaries 2007 and 2008) are examined.

[16] Because the thermal structure in the TTL is significantly affected by large-scale convective systems [e.g., *Eguchi and Shiotani*, 2004; *Kiladis et al.*, 2005; *Fujiwara et al.*, 2009, and references therein], it is important to survey the large-scale disturbances including convective activities during our campaign periods. Figure 3 shows the longitude-time distributions of temperature at 100 hPa and equivalent black body temperature (Tbb) averaged between 5°S and 5°N during the period from December 2006 to January 2007. Data are from the European Center for Medium-Range Weather Forecasts (ECMWF) operational analysis (with the vertical resolution of ∼400 m in the TTL) and from infrared images from the geostationary satellite MTSAT-1R, respectively. Figure 3 shows that an area with low Tbb values, i.e., active convection, moves eastward from ∼90°E at December 25 to ∼140°E at January 5 with the propagation speed of ∼6 m s^{-1}. This speed is close to the typical speed of MJO (∼5 m s^{-1} [e.g., *Eguchi and Shiotani*, 2004]). This convective system propagating eastward in the troposphere is regarded as the MJO. In the same figure, it is shown that at 100 hPa a warmer region, which is located to the west of the MJO convection, also propagates eastward at the similar speed to the MJO.

[17] Figure 4 shows the longitude-altitude distributions of temperature anomaly, zonal-vertical wind vectors, and potential temperature averaged between 5°S and 5°N on January 10, 2007. It is shown that there is a warm anomaly in the TTL that is tilted upward and eastward extending from 150 hPa over ∼90°E to 80 hPa over ∼140°E. There are also two cold anomalies, one at the upper west and the other at the lower east side of the tilted warm anomaly. The overall pattern propagates eastward as seen in Figure 3. These tilted thermal structures are dynamical response to the MJO heat source and well-documented features of the MJO [e.g., *Kiladis et al.*, 2005; *Fujiwara et al.*, 2009]. Over Kototabang, the tilted warm anomaly lowers the 360 K potential temperature surface and the upper west cold anomaly lifts the potential temperature surfaces of around 380–400 K. To the contrary, over Biak, the 360 K surface is lifted by the lower east cold anomaly and around 380 K surface are lowered by the tilted warm anomaly. The spatial and temporal relationship

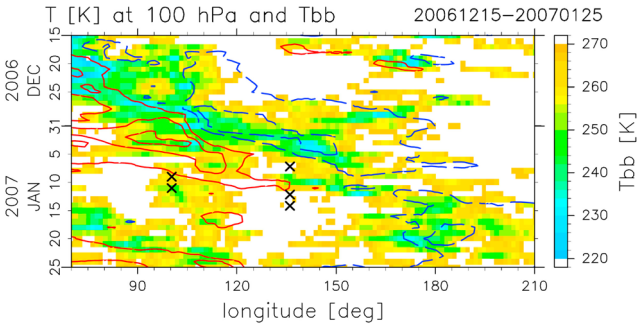

Figure 3. Longitude-time distributions of temperature anomaly at 100 hPa with respect to 191 K (contours with their interval 2 K: red solid lines (positive) and blue dashed lines (negative)) and equivalent black body temperature (Tbb) (colors) during the period from December 15, 2006 to January 25, 2007. Crosses indicate the sonde measurements.

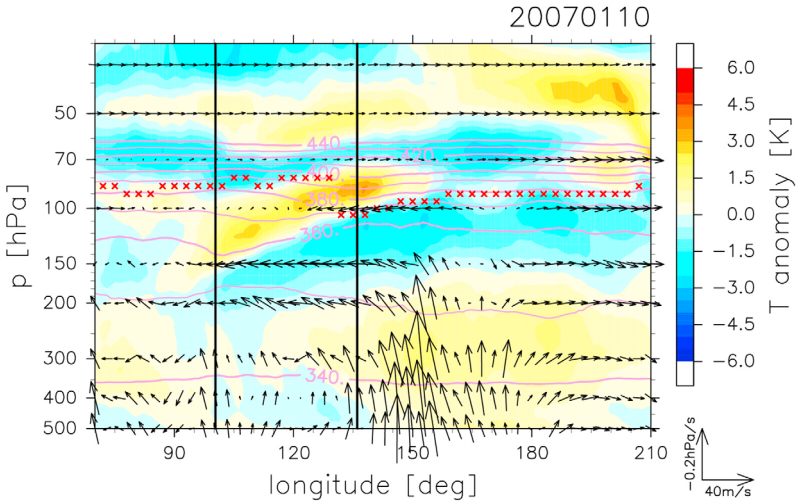

Figure 4. Longitude-altitude distributions of temperature anomaly with respect to zonal mean (colors), zonal and vertical wind vectors (arrows), and potential temperature (purple contours) on January 10, 2007. Vertical black lines indicate the locations of Kototabang (100.32°E) and Biak (136.06°E). Red crosses indicate the cold point tropopause locations.

between our measurements over the two sites and the phases of large-scale disturbances as described above are very similar for the other campaign in 2008 (not shown). These large-scale disturbances produce well-developed thick TTL over Kototabang and quite thin TTL over Biak, respectively, as also seen from our ozone measurements (Figures 2d and 2h).

[18] *Eguchi and Shiotani* [2004] revealed that cirrus clouds coexisted frequently with the cold anomaly at the east side of the tilted warm anomaly in association with the MJO. This is reconfirmed in this study as optically thick cirrus clouds over Biak. It is also suggested from our trajectory analysis that the cirrus clouds over Biak originate from convective outflow (not shown). In addition, our measurements suggest that high supersaturations inside thin cirrus clouds are formed at the west side of the MJO convective system and just below the cold point in the TTL when the potential temperature surfaces of around 380 K are lifted and the 360 K potential temperature surface is lowered by the large-scale disturbances.

[19] In this study, it is suggested that the differences between the two sites result from the phase difference of the large-scale disturbances such as MJO rather than the geographical difference. Furthermore, there is a strong possibility that the presence and degree of supersaturation depend on the phase of these disturbances such that optically thin (thick) cirrus clouds are formed with high (low) supersaturations at the upper west (lower east) side of the tilted warm anomaly in the thickened (thinned) TTL associated with the large-scale disturbances.

5. Concluding Remarks

[20] This study is the first to analyze relative humidity measured by balloon-borne CFH and collocated measurements of cirrus clouds using space-borne CALIOP sensors at two stations over the Indonesian maritime continent in January 2007 and 2008, coinciding with the coldest TTL. There are twelve sets of collocated measurements, five at Kototabang and seven at Biak. High supersaturations are often measured inside cirrus clouds. At Kototabang three out of five cases show supersaturation greater than 125% RHi with a maximum of about 160%. On the other hand, in Biak almost all cases which have cirrus clouds are unsaturated with lower concentrations of ozone. Analysis of background meteorological fields suggested a strong possibility that the presence and the degree of supersaturation depend on the phases of large-scale disturbances such as MJO rather than the geographical difference. Furthermore, it is suggested that optically thin (thick) cirrus clouds are formed with high (low) supersaturations at the upper west (lower east) side of the tilted warm anomaly in the thickened (thinned) TTL associated with the large-scale disturbances.

[21] **Acknowledgments.** We are thankful to the SOWER collaborators, especially M. Shiotani for constructive comments, and the collaborators of LAPAN of Indonesia. We also thank the CALIPSO/CALIOP team. The MTSAT-1R data are obtained from Kochi University. This work was supported by KAKENHI (15204043, 16740264, and 18204041) and Global Environment Research Fund of the Ministry of the Environment (A-1 and A-071). The figures were produced using the GFD-DENNOU Library. Comments by anonymous reviewers helped to improve the manuscript.

[22] The editor thanks two anonymous reviewers for assistance evaluating this manuscript.

References

Eguchi, N., and M. Shiotani (2004), Intraseasonal variations of water vapor and cirrus clouds in the tropical upper troposphere, *J. Geophys. Res.*, *109*, D12106, doi:10.1029/2003JD004314.

Fernald, F. G. (1984), Analysis of atmospheric lidar observations: Some comments, *Appl. Opt.*, *23*, 652–653.

Fujiwara, M., et al. (2009), Cirrus observations in the tropical tropopause layer over the Western Pacific, *J. Geophys. Res.*, *114*, D09304, doi:10.1029/2008JD011040.

Fujiwara, M., et al. (2010), Seasonal to decadal variations of water vapor in the tropical lower stratosphere observed with balloon-borne cryogenic frost point hygrometers, *J. Geophys. Res.*, *115*, D18304, doi:10.1029/2010JD014179.

Goff, A. J., and S. Gratch (1946), Low-pressure properties of water from −160 to 212°F, *Trans. Am. Soc. Heat. Vent. Eng.*, *52*, 95–122.

Hatsushika, H., and K. Yamazaki (2003), Stratospheric drain over Indonesia and dehydration within the tropical tropopause layer diagnosed by air parcel trajectories, *J. Geophys. Res.*, *108*(D19), 4610, doi:10.1029/2002JD002986.

Holton, J. R., and A. Gettelman (2001), Horizontal transport and the dehydration of the stratosphere, *Geophys. Res. Lett.*, *28*, 2799–2802.

Inai, Y., F. Hasebe, K. Shimizu, and M. Fujiwara (2009), Correction of radiosonde pressure and temperature measurements using simultaneous GPS height data, *SOLA*, *5*, 109–112, doi:10.2151/sola.2009-028.

Jensen, E. J., et al. (2008), Formation of large (≈100 μm) ice crystals near the tropical tropopause, *Atmos. Chem. Phys.*, *8*, 1621–1633.

Kiladis, G. N., K. H. Straub, and P. T. Haertel (2005), Zonal and vertical structure of the Madden-Julian oscillation, *J. Atmos. Sci.*, *62*, 2790–2809, doi:10.1175/JAS3520.1.

Krämer, M., et al. (2009), Ice supersaturations and cirrus cloud crystal numbers, *Atmos. Chem. Phys.*, *9*, 3505–3522.

List, R. J. (1984), *Smithsonian Meteorological Tables*, 5th ed., 350 pp., Smithsonian Inst., Washington, D. C.

Massie, S. T., J. Gille, C. Craig, R. Khosravi, J. Barnett, W. Read, and D. Winker (2010), HIRDLS and CALIPSO observations of tropical cirrus, *J. Geophys. Res.*, *115*, D00H11, doi:10.1029/2009JD012100.

Peter, T., C. Marcolli, P. Spichtinger, T. Corti, M. B. Baker, and T. Koop (2006), When dry air is too humid, *Science*, *314*, 1399–1402.

Shibata, T., H. Vömel, S. Hamdi, S. Kaloka, F. Hasebe, M. Fujiwara, and M. Shiotani (2007), Tropical cirrus clouds near cold point tropopause under ice supersaturated conditions observed by lidar and balloon-borne cryogenic frost point hygrometer, *J. Geophys. Res.*, *112*, D03210, doi:10.1029/2006JD007361.

Vaisala (1997), RS80 Radiosonde Technical Information, *Ref. A571en 1997-08*, 4 pp., Helsinki.

Vömel, H., D. David, and K. Smith (2007), Accuracy of tropospheric and stratospheric water vapor measurements by the cryogenic frost point hygrometer: Instrumental details and observations, *J. Geophys. Res.*, *112*, D08305, doi:10.1029/2006JD007224.

Wang, P., M. Patrick, M. M. Patrick, K. S. Geoffrey, and S. M. Kristi (1996), A 6-year climatology of cloud occurrence frequency from Stratospheric Aerosol and Gas Experiment II observations (1985–1990), *J. Geophys. Res.*, *101*(D23), 29,407–29,429, doi:10.1029/96JD01780.

Winker, D. M., W. H. Hunt, and M. J. McGill (2007), Initial performance assessment of CALIOP, *Geophys. Res. Lett.*, *34*, L19803, doi:10.1029/2007GL030135.

Wu, D. L., J. H. Chae, A. Lambert, and F. F. Zhang (2011), Characteristics of CALIOP attenuated backscatter noise: implication for cloud/aerosol detection, *Atmos. Chem. Phys.*, *11*, 2641–2654, doi:10.5194/acp-11-2641-2011.